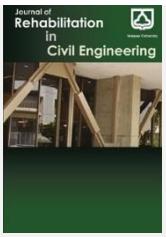

Journal of Rehabilitation in Civil Engineering

Journal homepage: https://civiljournal.semnan.ac.ir/

Effect of Near-Fault Earthquake Characteristics on Seismic Response of Mid-Rise Structures with Triple Friction Pendulum Isolator

Ali Majdi [1,*]; Mohammadreza Mashayekhi [2,*]; Ataallah Sadeghi-Movahhed [3]

1. Department of Building and Construction Techniques Engineering, Al- Mustaqbal University College, 51001 Hilla, Iraq
2. Assistant Professor, Department of Civil Engineering, K. N. Toosi University of Technology, Tehran, Iran
3. Department of Civil Engineering, Shabestar Branch, Islamic Azad University, Shabestar, Iran
* Corresponding authors: *alimajdi@uomus.edu.iq* (A.M.); *m.mashayekhi@kntu.ac.ir* (M.M.)

ARTICLE INFO

Article history:
Received: 22 April 2023
Revised: 03 June 2023
Accepted: 05 July 2023

Keywords:
Mid-rise building;
Triple friction pendulum isolator;
Near-Fault earthquakes;
Pulse characteristic.

ABSTRACT

Pulses of near-fault earthquakes are very effective in the seismic response of the Triple Friction Pendulum Isolator (TFPI). In previous studies, the effect of original bi-directional pulses components on the isolated tall buildings by TFPI was neglected. Also, the effect of changing the design parameters of TFPI on preventing seismic disaster in this type of building is unknown. For this reason, a 10 stories moment steel structure mounted on TFPI was designed. Then, the seven pairs of bidirectional near-fault earthquake records without and with removal pulses were applied to the isolated structure. The results show that the seismic responses on the base level decrease by reducing the velocity pulse amplitude (A_P) and increasing the velocity pulse period (T_P), also if the period of the isolators (T_M) is being higher than T_P, the seismic responses on the upper floors reduce. Moreover, Increasing the geometrical dimensions of the TFPI can significantly reduce the seismic effect of near-fault earthquake with pulses.

E-ISSN: 2345-4423

How to cite this article:
Majdi, A., Mashayekhi, M., & Sadeghi-Movahhed, A. (2024). Effect of Near-Fault Earthquake Characteristics on Seismic Response of Mid -Rise Structures with Triple Friction Pendulum Isolator. Journal of Rehabilitation in Civil Engineering, 12(1), 47-62. https://doi.org/10.22075/jrce.2023.30434.1845

1. Introduction

Seismic isolators are developing rapidly due to their high performance against ground motions. Numerous studies were evaluated the performance of different base isolation systems [1–5]. The single-pendulum friction isolator system is one of the common seismic isolators introduced by Zayas et al. [6]. After that, the double concave friction pendulum bearing was developed by Fenz and Constantinou [7]. This isolator was investigated theoretically and experimentally with a general look at the effect of changing the design parameters on the isolator behavior. Also, they have developed the Triple Friction Pendulum Isolator (TFPI) theoretically [8] and experimentally [9]. The TFPI consists of two concave plates, two articulated sliders, and a rigid slider in the middle that is assembled as a nested system. Figure 1 displays components of the TFPI. Majdi et al. [10] investigated the influence of unexpected earthquake severity on isolated structures using TFPI. The study found that structures designed for an earthquake hazard level with a return period of 475 years had a higher probability of collapse under an earthquake hazard level with a return period of 2475 years (MCER). Sadeghi-Movahhed et al. [11] developed a modified endurance time method for the dynamic analysis of isolated structures. The study demonstrated that this modified method provides better accuracy than the classic endurance time method when analyzing isolated structures using TFPI. Morgan and Mahin [12] have compared three classes of isolated buildings, including a classic linear viscous isolation system, a bilinear hysteretic isolation system, and the TFPI system for a shear-type structure under various intensity levels of the earthquake. They stated that the TFPI has the optimal behavior to reduce drift and acceleration.

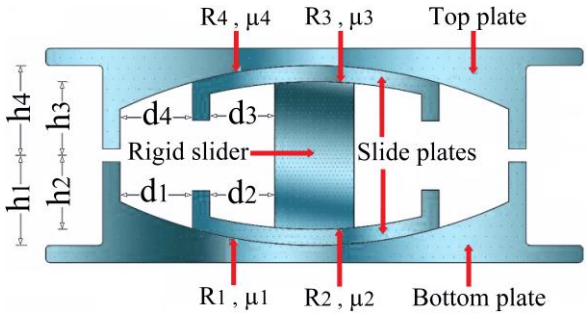

Fig. 1. Cross-section of triple friction pendulum isolator [10].

Becker and. Mahin [13] investigated the behavior of TFPI under bi-directional ground motions regardless of the superstructure effect. The study concluded that TFPI has high reliability against most lateral forces. Ryan and Dao [14] investigated the behavior of a 5-story moment frame building with TFPI using a three-dimensional shaking test. They concluded that the superstructure remains in the elastic stage, and the TFPI ability against the amplification of the horizontal acceleration has not diminished by the addition of vertical earthquake force. Dhankot and Soni [15] applied unidirectional far-field and near-fault ground motions with pulses on a five-story shear structure with TFPI. They concluded that the displacement, base shear, and absolute acceleration under near-fault ground motions are significantly more than far-field earthquakes. Also, increasing the radius of the outer surfaces (Figure 1) can decrease the base shear and absolute acceleration due to increases in the isolator displacement. Moeindarbari and Taghikhany [16] demonstrated that the outer surfaces of TFPI are more effective than the inner surfaces on the seismic responses of the structure under near-fault ground motions. Tajammolian et al. [17] investigated the effects of near-fault pulses earthquakes on a two-dimensional single-story structure with different types of friction pendulum isolators. They used the mathematical pulse model and concluded that the TFPI has better performance than other isolators against the effect of pulses. Previous research about the TFPI neglected the effect of

original pulses components on mid-rise superstructures and used the unidirectional mathematical pulses model to study the effect of pulses components. Also, the role of the TFPI de-sign parameters in reducing the effect of pulses of records in mid-rise isolated structures needs to be more investigated. These issues are investigated in the present study without the previous investigation simplifications.

For these aims, a mid-rise steel structure mounted on TFPI is designed with the Equivalent Lateral Force (ELF) process. The seismic responses of the designed structure are evaluated by the nonlinear time history method under near-fault earthquakes with pulses. In the next step, the geometrical dimensions of TFPI are increased and the structure is re-evaluated for the effect of the outer radius of TFPI on the improvement of seismic responses. Finally, the same ground motions with removal pulses are applied to the isolated structure, and the effect of near-fault earthquake components is investigated.

2. Force-Displacement relation of the TFPI

Fenz and Constantinou [8] assumed that the relation of the friction coefficient of surfaces is $\mu_2 = \mu_3 < \mu_1 < \mu_4$. The difference in the friction coefficient between the outer surface causes asynchronous slide on upper and lower surfaces and increases the regimes of the slide. Sarlis and Constantinou [18] replaced the above relation with $\mu_2 = \mu_3 < \mu_1 = \mu_4$. Indeed, they reduced the regimes from 5 to 3 that arise due to sliding on the outer surface simultaneously (Figure 2). This method has been used in many types of research [19–21] to study TFPI behavior.

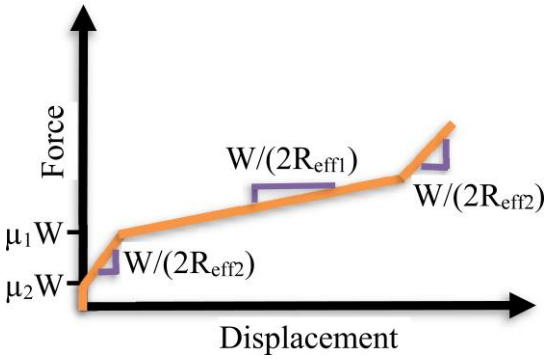

Fig. 2. Force-displacement relation of the triple friction pendulum isolator [10].

In Figure 3, the steps for sliding on surfaces and the displacement capacity for all regimes are presented based on $R_{eff\text{-}i}$ and d_i^* [20]:

$$R_{eff-i} = R_i - h_i \quad (1)$$

$$d_i^* = d_i \frac{R_{eff-i}}{R_i} \quad (2)$$

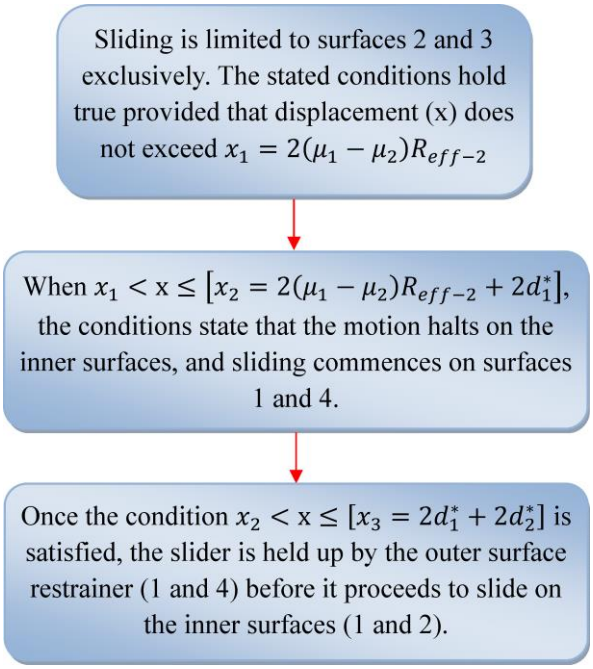

Fig. 3. Sliding steps on TFPI surfaces.

3. Design of the TFPI

The performance of the TFPI in the third regime (sliding on the outer surfaces) is better than other regimes [22]. In the design process, TFPI is prevented from entering the fifth regime. Because in the fifth regime, the slide on outer surfaces reached their maximum displacement capacity, and only inner surfaces have some capacity to slide. Also, this regime

does not decrease the transitional force to the superstructure [23]. The behavior of the TFPI in the last regime is similar for both 3-regimes and 5-regimes conditions. Therefore, the TFPI is designed for the second regime base on the 3-regimes conditions in the present study.

According to the ASCE7-16 [24] code, the ELF procedure can be used to obtain the isolator design values. In the ELF procedure, D_M is estimated initially. Then K_M, T_M, and β_M calculated using the following formulas:

$$K_M = F/D_M \quad (3)$$

$$T_M = 2\pi\sqrt{\frac{W}{K_M g}} \quad (4)$$

$$\beta_M = \frac{\sum E_M}{2\pi D_M^2 K_M} \quad (5)$$

Finally, the maximum estimated displacement controls by equation (6). If there is a large difference, the steps above will be re-calculated.

$$D_M = \frac{g S_{M1} T_M}{4\pi^2 B_M} \quad (6)$$

T_M is considered greater than three times the elastic fixed-base period of the superstructure (T_{fix}) in the design process (Table. 1) according to ASCE7-16 [24].

In this study, the geometric properties of the TFPI1 and TFPI2 are chosen according to the defined process by Constantinou et al. [19] and illustrated in Table 1. TFPI1 is used to design and evaluate the isolated structure according to the aims of the study, while TFPI2 is only used in the assessment process. TFPI1 and TFPI2 differ in the size of their outer surfaces, which affects their displacement capacity and, in turn, increases T_M. While there is only a slight difference in displacement capacity, the enhancements to the outer surfaces have a significant impact on T_M.

Mokha et al. [25] and Mokha et al. [26] investigated the frictional properties and effective factors on the base isolation with Teflon bearing by experimental study. Also, Constantinou et al. [27] introduced a mathematical model to calculate the coefficient of friction. Constantinou et al. [19] presented the following formulas for the TFPI with a pressure (p) limitation on the isolator.

$$\mu_{3C} = 0.122 - 0.01p \quad (7)$$

$$\mu_{1C} = 1.2\mu_{3C} \quad (8)$$

In these formulas, the μ_{1C} is calculated based on the μ_{3C}. The pressure range on the isolator for a logical answer is determined between 13.8 to 55.2 MPa. Also, it is necessary to reduce the value obtained for the μ_{3C} in large-size isolators and velocities of around 1 m/s by about 0.01 to 0.02 [19]. The obtained coefficient of friction for each surface of the TFPI is for high-speed conditions (Table 1). Also, half of these are considered for low-speed conditions.

Table 1. Properties of the TFPI.

	$R_{1eff} = R_{4eff}$ (m)	$R_{2eff} = R_{3eff}$ (m)	$d_1 = d_4$ (m)	$d_2 = d_3$ (m)	$\mu_1 = \mu_4$	$\mu_2 = \mu_3$	T_{fix} (sec)	T_M (sec)
TFPI1	3.81	0.66	0.7	0.2	0.087	0.071	1.2	4.28
TFPI2	5.85	0.66	0.8	0.2	0.087	0.071	1.2	4.9

4. Superstructure

In this research, a three-dimensional 10-story steel moment frame building (Figure 4) is designed by AISC360-16 [28], AISC 341 [29], and ASCE7-16 [24]. The Sap2000 software [30] is used to design and evaluate the structure. There are three bays in each principal horizontal direction which each bay length is 6m and the height of each floor is 3.2m. The cross-sections of the beams and columns are W-shape and Box, respectively. The dimensions and mechanical characteristics are presented in Tables 2 and 3. Applied dead

loads to floors and roof are 6 kN/m^2 and 4 kN/m^2, respectively, while the live loads on floors and roof are 2 kN/m^2 and 1.5 kN/m^2, respectively.

Table 2. cross-sections of the beams and columns.

Story	1-3	4-7	8-10
Column(cm)	BOX45×2	BOX35×2	BOX30×1.5
Beam	W12×170	W12×96	W12×50

The direct integration method in Sap2000 [30] takes into account the nonlinear effect of plastic hinged elements. However, this method may cause uncontrolled fluctuation in the damping of the TFPI. Therefore, Sarlis and Constantinou [18] have recommended that the damping of the superstructure specifies as zero. Accordingly, nonlinear time history analysis considering zero superstructure damping is used for evaluating the structure.

Table 3. Material properties of steel sections.

Yield stress (MPa)	Ultimate Stress (MPa)	Poisson's ratio	Young's modulus (MPa)
345MPa	448.16MPa	0.3	2×10^5MPa

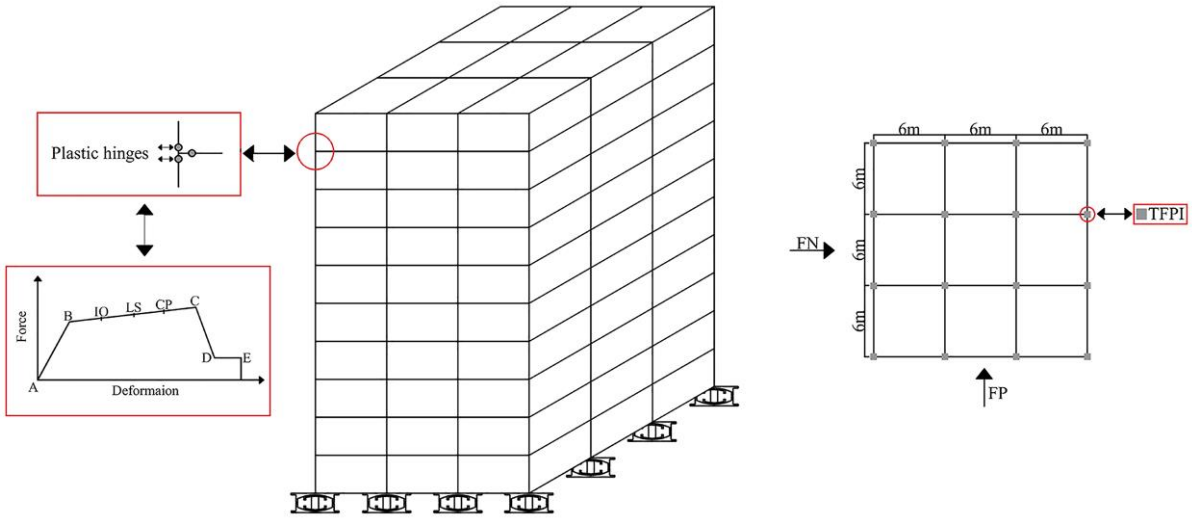

Fig. 4. Illustration of the building model and defined the generalized force–deformation curve of plastic hinges.

In some investigations of the seismic isolator [31], the superstructure is assumed to remain in the elastic stage. This assumption may not be correct in some conditions, such as increasing the height of the building, changing the soil type, and the conditions of the zone faults. ASCE41-17 [32] defined a generalized Force–deformation relation curve for considering the nonlinear behavior of steel elements (Figure 4). Also, this has specified three-level including Immediate Occupancy (IO), Life Safety (LS), and Collapse Prevention (CP) with their values for evaluating the performance of the superstructure. Coefficients of the deformational moment-rotation plastic hinges and acceptance criteria of this for beams and columns are selected from ASCE41-17 [32] and applied to sap2000 [30].

5. Ground motions

According to ASCE7-16 [24], the nonlinear time history analysis of seismic isolators should be conducted under the MCE_R. To meet this requirement, seven pairs of records with pulses (Table 4) were selected from the list provided by Baker et al. [33]. These records are related to soil type D, with pulse periods ranging from 1.2s to 4.6s. The records were downloaded from the Pacific Earthquake Engineering Research Center [34] database.

Table 4. Characteristics of ground motion records.

No.	Event	Station	year	M_w	R_{rup} (km)	V_{s30} (m/s)	T_P (sec)
1	Imperial Valley-06	El Centro Array#4	1979	6.53	7.05	208.91	4.6
2	Imperial Valley-06	El Centro Array#5	1979	6.53	3.95	205.63	4
3	Imperial Valley-06	El Centro Array#6	1979	6.53	1.35	203.22	3.8
4	Imperial Valley-06	El Centro Array#7	1979	6.53	0.56	210.51	4.2
5	Northridge-01	Newhall – W Pico Canyon Rd	1994	6.69	5.48	285.93	2.4
6	Northridge-01	Rinaldi Receiving Sta	1994	6.69	6.5	282.25	1.2
7	Chi-Chi, Taiwan	CHY101	1999	7.62	9.94	258.89	4.6

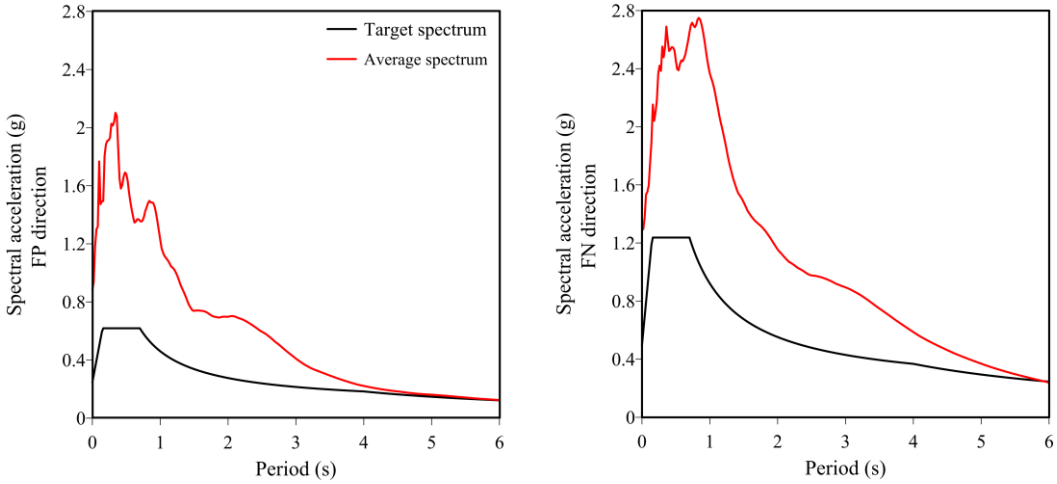

Fig. 5. The scaled mean acceleration spectra in the FN and FP directions.

ASCE7-16 [24] proposed amplitude scaling and spectral matching methods for modifying ground motions. In this study, the amplitude scaling method is used (Figure 5) because it maintains the frequency characteristics of the original records [35]. Selected ground motions are scaled to 100% and 50% of the MCE_R spectrum in the Fault-Normal (FN) and Fault-Parallel (FP) directions, respectively. The different MCER spectrum levels for scaling in the orthogonal directions are used because the records are obtained from sites within 5 km of the active fault. The average spectrum of each pair of components is scaled for the period range of $0.2T_M$ to $1.25T_M$ [24].

Because of the symmetric structure, the variety of seismic responses in the principal horizontal directions of the structure depends solely on the different horizontal ground motion acceleration components. Therefore, the component direction of records that are applied perpendicular to the structural sides is used in the result discussion.

The evaluation is conducted in two steps. First, bidirectional ground motions are applied to the structure in its original mode, and the structure is evaluated. Second, the same records with the pulses removed are used in the analysis, and the results are compared to those of the first step.

6. Results

6.1. Interstory drift ratio

The average inter-story drift ratio of the floors is presented in Figure 6. This demonstrates that both isolators kept the average drift ratio within acceptable limits (less than 2%), according to ASCE 7-16 [24]. The TFPI2 system was able to reduce the average drift ratio of each story more than the TFPI1 under earthquakes with pulses due to the larger geometrical dimensions. The TFPI2 has decreased the average drift ratio by about 35.7%-44.8% and 1.2%-25.2% more than the TFPI1 in the FN and FP directions, respectively. Similar behavior can be seen in most of the records. For example, the TFPI2 has decreased the drift ratio by about 18.64%-52.47% and 2.87%-38.67% more than the TFPI1 under the Imperial Valley- Array#6 (Figure 7) and Northridge-Rinaldi (Figure 8) ground motions, respectively. However, the performance of the TFPI1 on some floors is better than TFPI2 under the FP direction of the Chi-Chi earthquake (Figure 9).

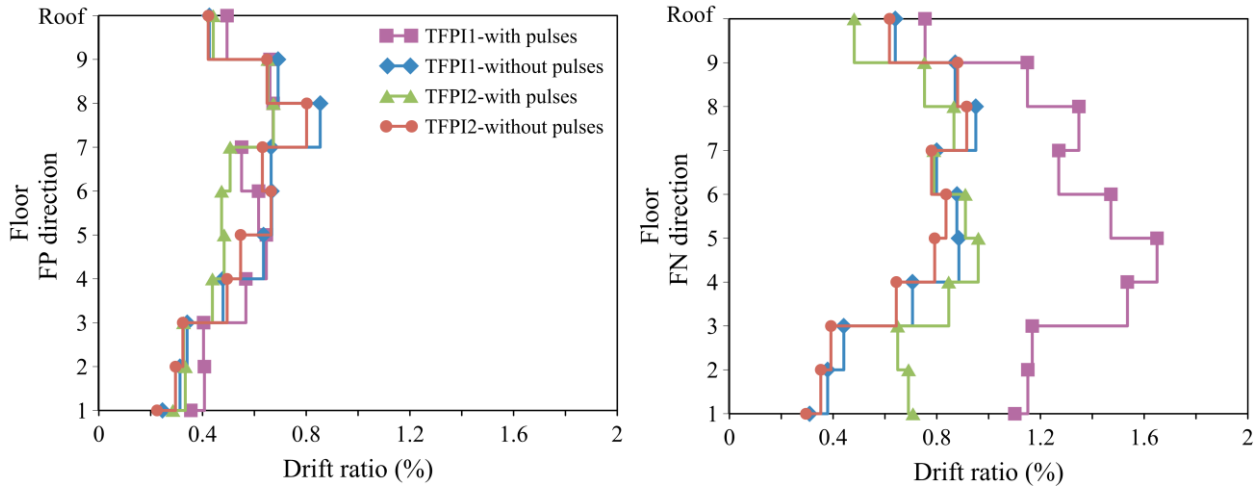

Fig. 6. Average inter-story drift ratio of the floors.

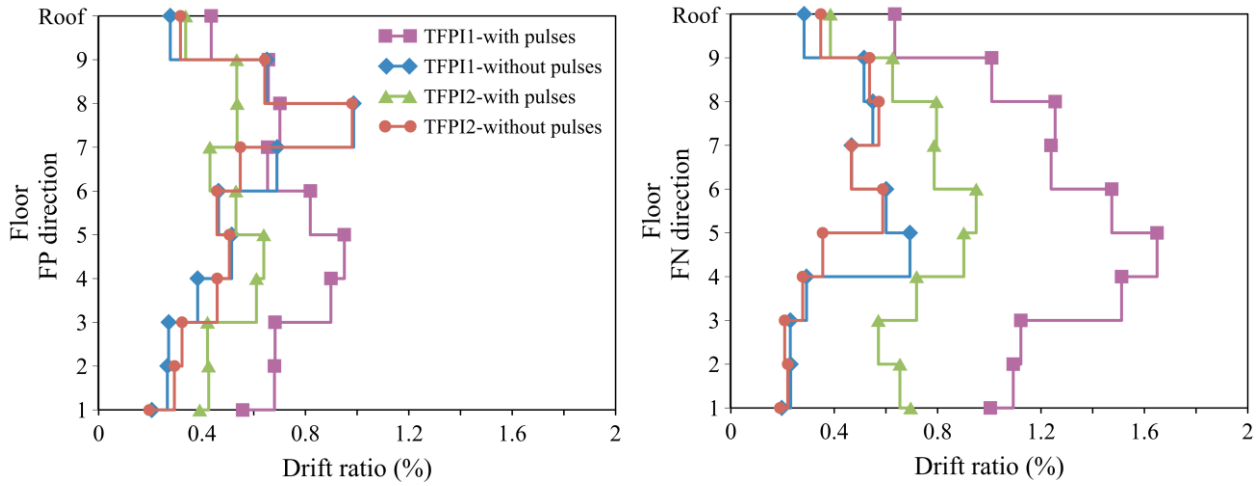

Fig. 7. Peak drift ratio subjected to Imperial Valley-Array#6 ground motion.

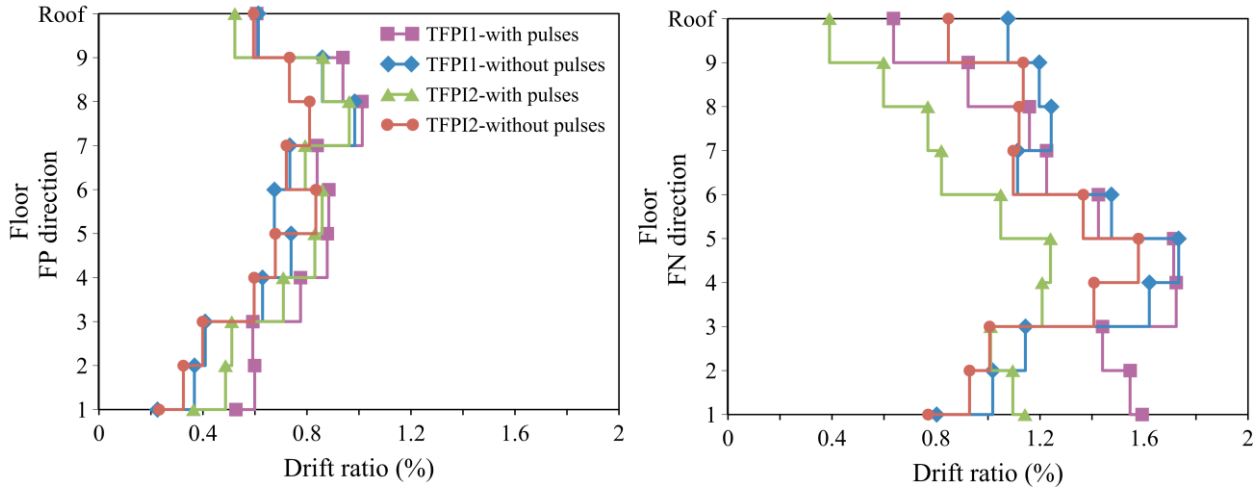

Fig. 8. Peak drift ratio subjected to Northridge-Rinaldi ground motion.

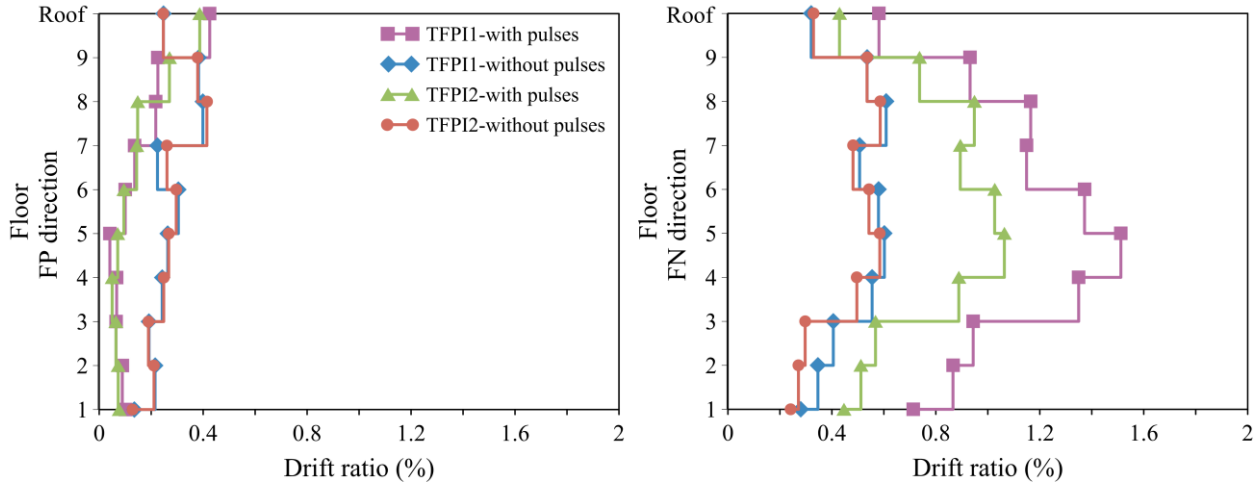

Fig. 9. Peak drift ratio subjected to Chi-Chi ground motion.

Under earthquake conditions without pulses, TFPI2 shows better performance than TFPI1 in reducing the average inter-story drift ratio by 0.3%-13.88% on most floors. However, the positive effect of TFPI2 is reduced or even eliminated on some floors. For example, TFPI1 reduces the average inter-story drift ratio of the 9th floor in the FN direction and the 4th floor in the FP direction by 1.1% and 3.3% more than TFPI2 (Figure 6). This may be due to the removal of the pulse and the decrease in earthquake intensity.

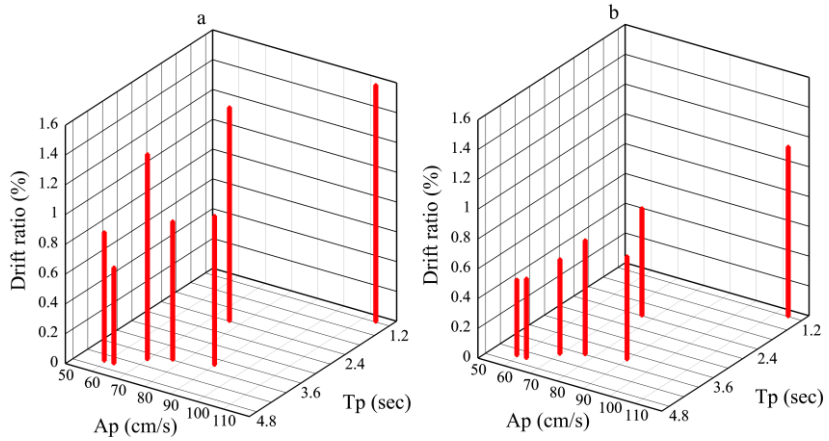

Fig. 10. Correlation of peak drift ratio with pulses characteristics subjected to story 1 in the FN direction: a) TFPI1; b) TFPI2.

The highest value of the velocity pulse amplitude (A_p) and the lowest value of the T_P are effective in the enhancement of drift ratio at the lower floors for both isolators (Figure 10). So that, the Northridge-Rinaldi earthquake has the maximum drift ratio in comparison to other earthquakes with the lowest value of T_P equal to 1.2 seconds and the highest value of A_P equal to 114.87 cm/s on the 1st floor. On the other hand, the maximum value of T_P, which is smaller than T_M, and the corresponding A_P are more effective on upper floors for both isolators (Figure 11). So that, the Imperial Valley- Array#7 has the maximum drift ratio on the 9th story which T_P is equal to 4.2 seconds and the A_P is equal to 70 cm/s.

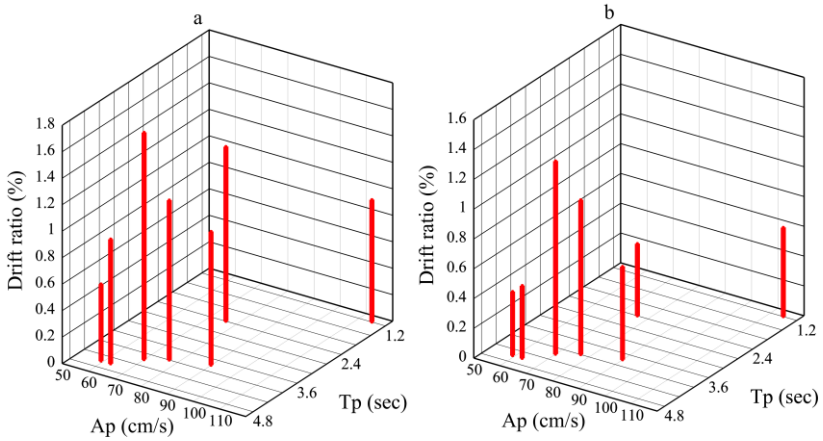

Fig. 11. Correlation of peak drift ratio with pulses characteristics subjected to story 9 in the FN direction: a) TFPI1; b) TFPI2.

6.2. Acceleration response of stories

The average absolute acceleration of ground motions with and without pulses for both isolators is shown in Figure 12. In addition, the maximum absolute acceleration of floors under Northridge-Rinaldi and Imperial Valley-Array #4 ground motions is plotted in Figures 13 and 14, respectively. It is clear that the TFPI2 can reduce the average acceleration of ground motions with pulses more than the TFPI1. However, a comparison of records individually shows that different results could occur. For example, the TFPI1 has better performance on the upper floors about 81%-150% under the FP direction of the Imperial Valley-Array#4 (Figure 14).

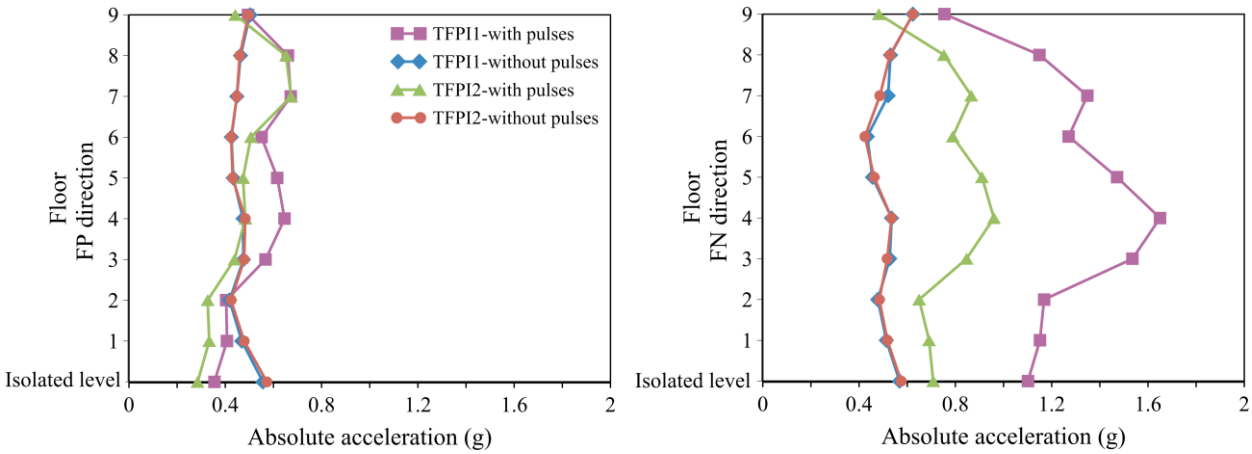

Fig. 12. Average absolute acceleration of the floors.

Removing pulses can have a negative effect under some records. Therefore, both isolators have poor performance on the upper and lower floors under Northridge-Rinaldi ground motion (Figure 13). Similarly, all floors have experienced higher absolute acceleration in the FP direction of Imperial Valley-Array #4 ground motion with removal pulses (Figure 14).

The performance of isolators is almost close to each other under records without pulses. Indeed, it was predicted that the TFPI2 would perform better than the TFPI1 by removing the pulse. Still, it seems that pulse removal from the earthquake has reduced ground motion severity, which has led to the equalization results for the isolators.

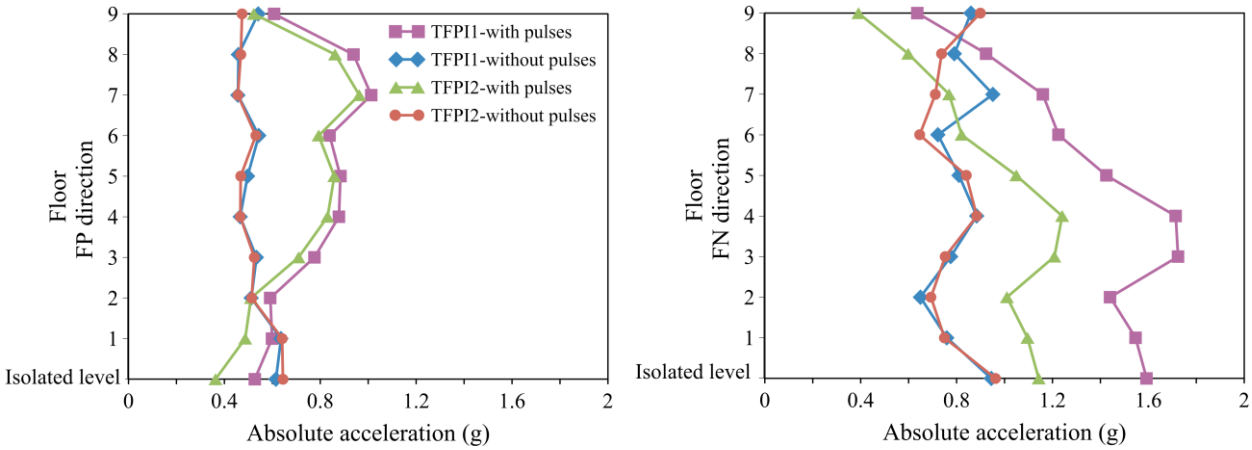

Fig. 13. Peak absolute acceleration subjected to Northridge-Rinaldi ground motion.

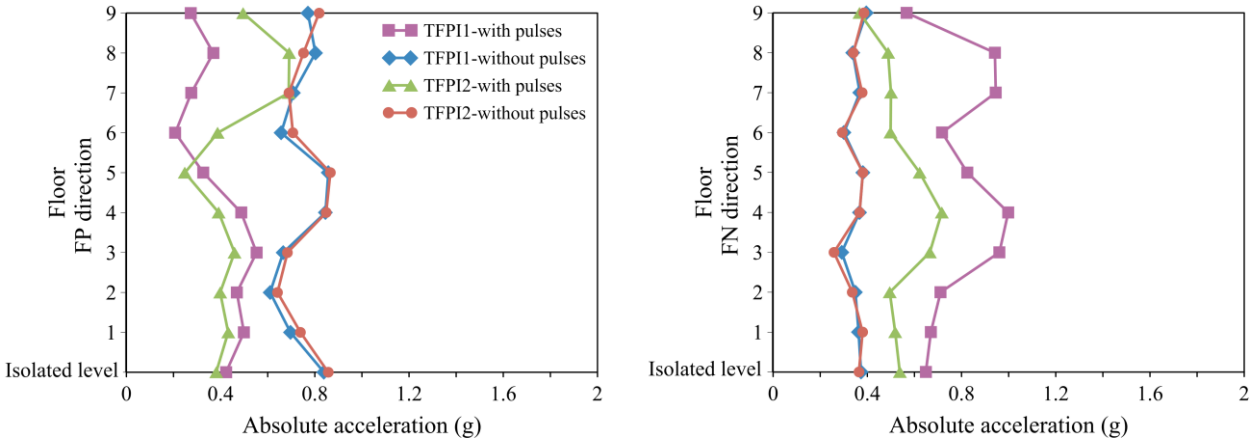

Fig. 14. Peak absolute acceleration subjected to Imperial Valley-Array #4 ground motion.

The effects of pulses components on the first and ninth floors are shown in Figures 15 and 16. The results are similar to the effect of pulses on the drift ratio. So that, the isolated structure has maximum absolute acceleration on the first story under the Northridge-Rinaldi earthquake with the highest A_P and lowest T_p. Also, this happens on the ninth story under the Imperial Valley- Array#7 earthquake with the highest T_P smaller than T_M and the corresponding A_P.

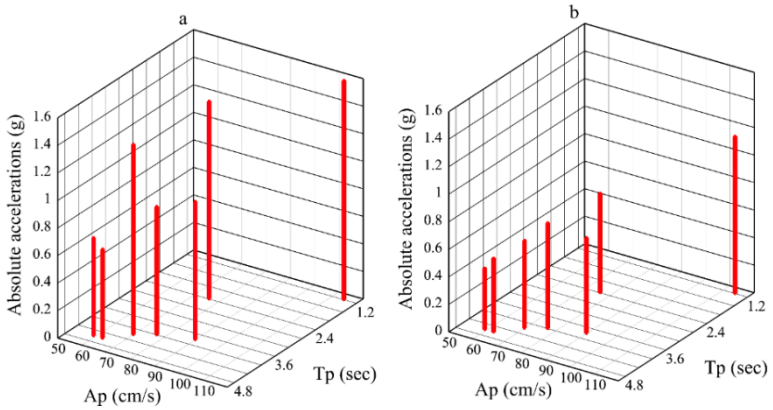

Fig. 15. Correlation of peak absolute acceleration with pulses characteristics subjected to story 1 in the FN direction: a) TFPI1; b) TFPI2.

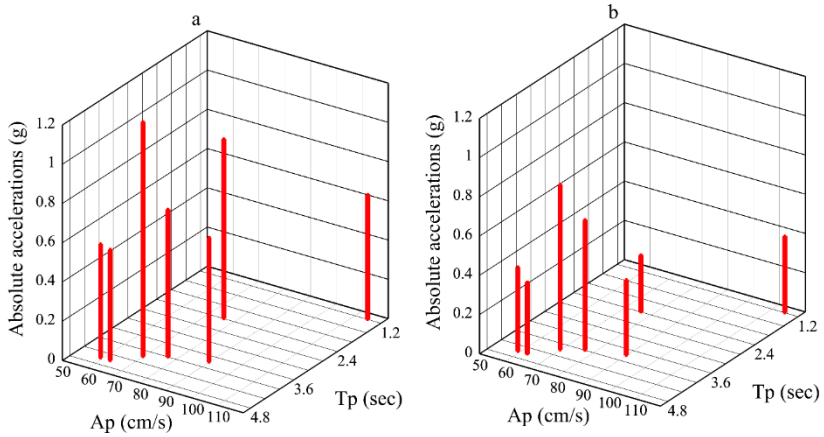

Fig. 16. Correlation of peak absolute acceleration with pulses characteristics subjected to story 9 in the FN direction: a) TFPI1; b) TFPI2.

6.3. Base shear

The normalized base shear value of all ground motions with their average is presented in Figure 17. The TFPI2 can reduce the average base shear force more than TFPI1 by about 22.31% and 7.92% under the FN and FP directions of the ground motions with pulses, respectively. However, TFPI1 performance is slightly better than TFPI2 under Imperial Valley-Array #4, Northridge-Rinaldi, and Chi-Chi earthquakes in the FP direction. The advantage of TFPI2 compares to TFPI1 increases under the FN direction of records that the FN direction is stronger than the FP direction.

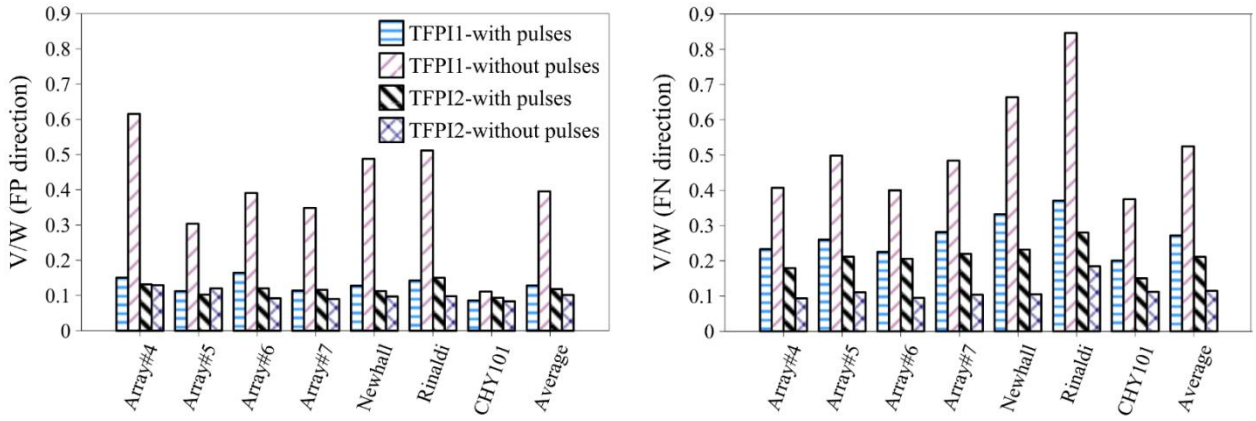

Fig. 17. The ratio of the base shear to the total weight of the structure (V/W).

Removing the pulse of records has a negative effect on the performance of the TFPI1. This increased the average base shear of the earthquakes without pulses by about 93% and 208% compared to earthquakes with pulses in the FN and FP directions, respectively. In contrast, removing the pulse had a positive effect on TFPI2 system performance. TFPI2 reduced the average base shear of the earthquakes without pulses compared to pulses by about 45.6% and 14.1% in the FN and FP directions. Individual study of records shows that TFPI2 reduces the base shear from 24.8% to 84.22% more than TFPI1.

It can be seen in Figure 18 that minimum base shear is related to the Chi-Chi earthquake with the highest T_P and lowest A_P compared to other ground motions. In contrast, the Northridge-Rinaldi earthquake with the highest A_P and lowest T_P caused maximum base shear.

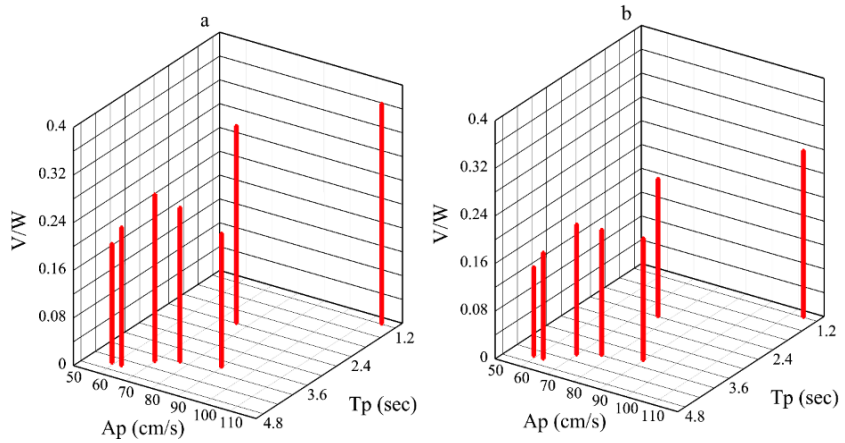

Fig. 18. Correlation of the ratio of the base shear to the total weight of the structure (V/W) with pulses characteristics in the FN direction: a) TFPI1; b) TFPI2.

6.4. Overturning moment

The maximum overturning moment of the base level for all records with their average are presented in Figure 19. The average response of records with pulses shows that TFPI2 has a better performance than TFPI1 for both directions. The TFPI2 decreases the average overturning moment more than TFPI1 by about 2.8% and 10% in the FN and FP directions, respectively. The individual study of records shows similar behavior for all of them.

In the isolated structure with TFPI1, removing the pulse from the records increased the overturning moment by about 21.15% and 9.7% in the FN and FP directions, respectively. In the isolated structure with TFPI2, removing the pulse decreased the overturning moment by about 1.4% and 4% in the FN and FP directions. Similar behavior has been observed under most of the records, except for the FN direction of the Chi-Chi and the FP direction of Imperial Valley-Array#4, 5, and 6 that TFPI1 decreased the overturning moment by about 13%, 7.9%, 5.8%, and 6.8%, respectively.

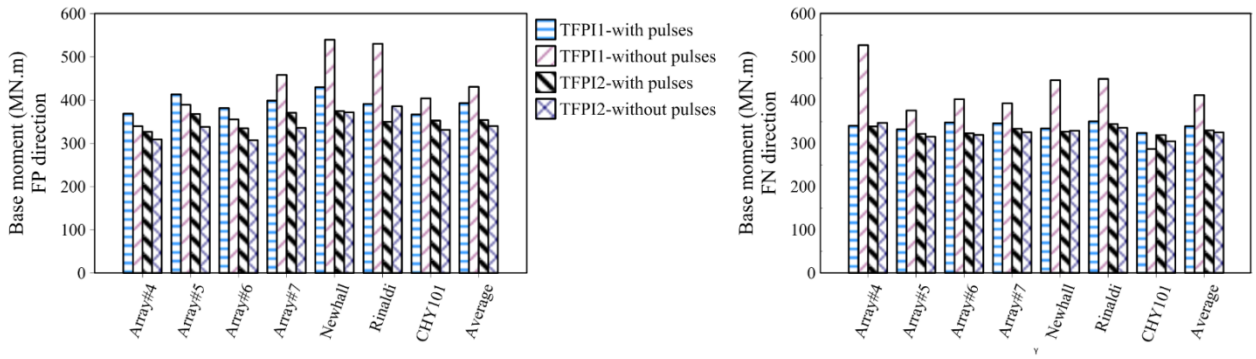

Fig. 19. Overturning moment subjected to all of the ground motions in base level.

The peak overturning moments increased with the enhancement of A_P and T_P reduction at the base level, as shown in Figure 20. The Northridge-Rinaldi earthquake with the highest A_P and lowest T_P, and the Chi-Chi earthquake with the highest T_P and lowest A_P caused maximum and minimum overturning moments values, respectively.

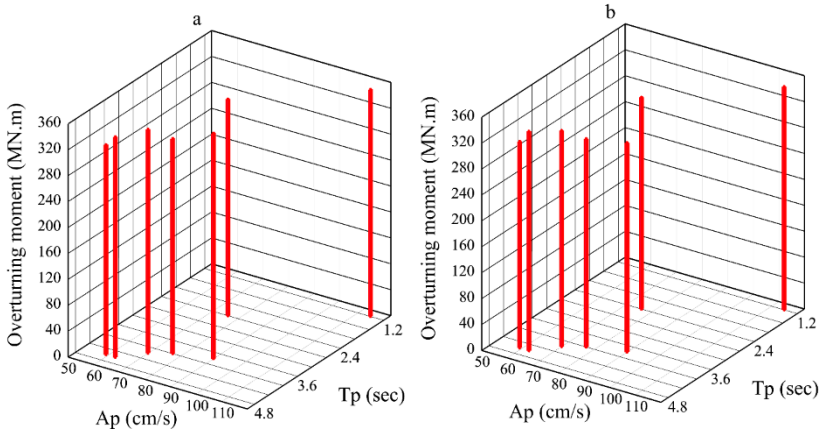

Fig. 20. Correlation of peak overturning moment of the base with pulses characteristics in the FN direction: a) TFPI1; b) TFPI2.

7. Conclusions

This study evaluated the performance of the TFPI on a mid-rise steel moment frame building with different geometry conditions under earthquakes with and without pulses. To achieve this, 2 types of TFPI were considered. The main difference between the 2 types of TFPI is the geometry of outer surfaces that leads to different periods. a 10-story building isolated by TFPI was subjected to a set of bi-directional near-fault pulse-type and removal pulses ground motions. The isolated building was analyzed using the nonlinear time history method, and the following results were obtained:

- Increasing the geometrical capacity of the isolator had a positive effect on the seismic behavior of isolated structure against ground motions with pulses and caused more reduction in the base shear, absolute acceleration, and drift ratio on most of the floors. But the effect of this advantage decreases for the overturning moment of the base.

- The performance of the isolators is very close to each other in reducing the acceleration under earthquakes without pulses, so increasing the dimensions of the isolator was not very effective in this. It seems that this close performance happens when the effect of acceleration

in stories is not high. In contrast, other structural seismic responses such as base shear, drift ratio, and the overturning moment of the base improved by increasing the geometrical dimensional of the isolator.

- The maximum A_P and minimum T_P lead to the highest drift ratio, overturning moment, base shear, and absolute acceleration on the lower floors under records with pulses. But this situation reverses as the height increases if the T_P is less than T_M.

This article did not consider the effect of the irregular plan. In addition, only the effect of the pulse of the near-fault forward directive earthquakes was investigated. Therefore, more research is needed to investigate the effect of irregular plan and pulse of fling step near-fault earthquakes on the behavior of the TFPI.

Symbols and abbreviations

R_i is the radius of each curvature
μ_i is the coefficient of friction between the surfaces
h_i is the height of each surface to the center of the rigid slider
d_i is the nominal displacement capacity
g is the acceleration due to gravity
μ_{1C} is the coefficient of friction in the first cycle
μ_{3C} is the coefficient of friction of the first three cycles
$R_{eff\text{-}i}$ is the effective radius of each curvature
d_i^* is the actual displacement capacities of each sliding surface
D_M is the maximum displacement at the center of rigidity of the isolation system
K_M is the effective stiffness of the isolation system in the horizontal direction
T_M is the effective period of the seismically isolated structure
β_M is the effective damping of the isolation system
W is effective seismic weight of the superstructure
$\sum E_M$ is total energy dissipated in the isolator during a full cycle
S_{M1} is the MCE_R, 5% damped, spectral response acceleration parameter at a period of 1-s
B_M is numerical coefficient for effective damping

Funding

This research received no external funding.

Conflicts of Interest

The authors declare that they have no conflict of interest.

Authors contribution statement

Ali Majdi: Conceptualization, Formal analysis, Investigation, Methodology, Software, Supervision, Validation, Writing – original draft, Writing – review & editing.
Mohammadreza Mashayekhi: Conceptualization, Investigation, Methodology, Software, Supervision, Writing – original draft, Writing – review & editing, Validation.
Ataallah Sadeghi-Movahhed: Conceptualization, Investigation, Methodology, Validation, Writing – review & editing.

References

[1] Mansouri S. The investigation of the effect of using energy dissipation equipment in seismic retrofitting an exist highway RC bridge subjected to far-fault earthquakes. Int J Bridg Eng 2021;9:51–84.
[2] Mansouri S, Kontoni DPN, Pouraminian M. The effects of the duration, intensity and magnitude of far-fault earthquakes on the

seismic response of RC bridges retrofitted with seismic bearings. Adv Bridg Eng 2022;3:19. https://doi.org/10.1186/s43251-022-00069-8.

[3] Mansouri S, Nazari A. The Effects of Using Different Seismic Bearing on the Behavior and Seismic Response of High-Rise Building. Civ Eng J 2017;3:160–71. https://doi.org/10.28991/cej-2017-00000082.

[4] Kuvat A, Sadoglu E, Zardari S. Experimental Investigation of Sand–Rubber–Bitumen Mixtures as a Geotechnical Seismic Isolation Material. Int J Geomech 2024;24:319–34. https://doi.org/10.1061/IJGNAI.GMENG-7015.

[5] Movahhed AS, Zardari S, Şadoğlu E. Seismic performance of a building base-isolated by TFP susceptible to pound with a surrounding moat wall. Earthquakes Struct 2022;23:723–36. https://doi.org/10.12989/eas.2022.23.1.723.

[6] Zayas VA, Low SS, Mahin SA. A Simple Pendulum Technique for Achieving Seismic Isolation. Earthq Spectra 1990;6:317–33. https://doi.org/10.1193/1.1585573.

[7] Fenz DM, Constantinou MC. Behaviour of the double concave Friction Pendulum bearing. Earthq Eng Struct Dyn 2006;35:1403–24. https://doi.org/10.1002/eqe.589.

[8] Fenz DM, Constantinou MC. Spherical sliding isolation bearings with adaptive behavior: Theory. Earthq Eng Struct Dyn 2008;37:163–83. https://doi.org/10.1002/eqe.751.

[9] Fenz DM, Constantinou MC. Spherical sliding isolation bearings with adaptive behavior: Experimental verification. Earthq Eng Struct Dyn 2008;37:185–205. https://doi.org/10.1002/eqe.750.

[10] Majdi A, Sadeghi-Movahhed A, Mashayekhi M, Zardari S, Benjeddou O, De Domenico D. On the Influence of Unexpected Earthquake Severity and Dampers Placement on Isolated Structures Subjected to Pounding Using the Modified Endurance Time Method. Buildings 2023;13:1278. https://doi.org/10.3390/buildings13051278.

[11] Sadeghi Movahhed A, Shirkhani A, Zardari S, Mashayekhi M, Noroozinejad Farsangi E, Majdi A. Modified endurance time method for seismic performance assessment of base-isolated structures. J Build Eng 2023;67:105955. https://doi.org/10.1016/j.jobe.2023.105955.

[12] Morgan TA, Mahin SA. Achieving reliable seismic performance enhancement using multi-stage friction pendulum isolators. Earthq Eng Struct Dyn 2010;39:1443–61. https://doi.org/10.1002/eqe.1043.

[13] Becker TC, Mahin SA. Experimental and analytical study of the bi-directional behavior of the triple friction pendulum isolator. Earthq Eng Struct Dyn 2012;41:355–73. https://doi.org/10.1002/eqe.1133.

[14] Ryan KL, Dao ND. Influence of Vertical Ground Shaking on Horizontal Response of Seismically Isolated Buildings with Friction Bearings. J Struct Eng 2016;142. https://doi.org/10.1061/(ASCE)ST.1943-541X.0001352.

[15] Dhankot MA, Soni DP. Behaviour of Triple Friction Pendulum isolator under forward directivity and fling step effect. KSCE J Civ Eng 2017;21:872–81. https://doi.org/10.1007/s12205-016-0690-3.

[16] Moeindarbari H, Taghikhany T. Seismic optimum design of triple friction pendulum bearing subjected to near-fault pulse-like ground motions. Struct Multidiscip Optim 2014;50:701–16. https://doi.org/10.1007/s00158-014-1079-x.

[17] Tajammolian H, Khoshnoudian F, Talaei S, Loghman V. The effects of peak ground velocity of near-field ground motions on the seismic responses of base-isolated structures mounted on friction bearings. Earthquakes Struct 2014;7:1159–282. https://doi.org/https://doi.org/10.12989/eas.2014.7.6.1259.

[18] Sarlis AA, Constantinou MC. Modeling triple friction pendulum isolators in program SAP2000. The technical report released to the engineering community. New York: 2010.

[19] Constantinou, M.C. Kalpakidis I, Filiatrault A, Ecker Lay RA. LRFD-Based Analysis and Design Procedures for Bridge Bearings and Seismic Isolators: MCEER-11-0004. Buffalo, NY, USA: 2011.

[20] McVitty WJ, Constantinou MC. Property modification factors for seismic isolators:

design guidance for buildings: MCEER-15-0005. Buffalo, NY, USA: 2015.

[21] Oikonomou, K. Constantinou MC, Reinhorn AM, Kempner L. Seismic isolation of high voltage electrical power transformers: MCEER-16-0006. Buffalo, NY, USA: 2016.

[22] Amiri GG, Namiranian P, Amiri MS. Seismic Response of Triple Friction Pendulum Bearing under Near-Fault Ground Motions. Int J Struct Stab Dyn 2015;16:1550021. https://doi.org/10.1142/S0219455415500212.

[23] Becker TC, Bao Y, Mahin SA. Extreme behavior in a triple friction pendulum isolated frame. Earthq Eng Struct Dyn 2017;46:2683–98. https://doi.org/https://doi.org/10.1002/eqe.2924.

[24] ASCE/SEI 7-16. Minimum design loads for buildings and other structures. American Society of Civil Engineers, Reston, VA: 2017.

[25] Mokha A, Constantinou M, Reinhorn A. Teflon Bearings in Base Isolation I: Testing. J Struct Eng 1990;116:438–54. https://doi.org/10.1061/(ASCE)0733-9445(1990)116:2(438).

[26] Mokha A, Constantinou M, Reinhorn A. Further Results on Frictional Properties of Teflon Bearings. J Struct Eng 1991;117:622–6. https://doi.org/10.1061/(ASCE)0733-9445(1991)117:2(622).

[27] Constantinou M, Mokha A, Reinhorn A. Teflon Bearings in Base Isolation II: Modeling. J Struct Eng 1990;116:455–74. https://doi.org/10.1061/(ASCE)0733-9445(1990)116:2(455).

[28] ANSI/AISC 360-16. Specification for Structural Steel Buildings. American Institute of Steel Construction: Chicago, IL: 2016.

[29] ANSI/AISC 341-16. Seismic Provisions for Structural Steel Buildings. American Institute of Steel Construction: Chicago, IL: 2016.

[30] Computers and Structures Inc. (CSI). SAP2000, Integrated Solution for Structural Analysis and Design. Berkeley, CA, USA: 2015.

[31] Sadeghi Movahhed A, Shirkhani A, Zardari S, Noroozinejad Farsangi E, Karimi Pour A. Effective range of base isolation design parameters to improve structural performance under far and near-fault earthquakes. Adv Struct Eng 2022;26:52–71. https://doi.org/10.1177/13694332221119870.

[32] ASCE/SEI 41-17. Seismic Evaluation and Retrofit of Existing Buildings. American Society of Civil Engineers, Reston, VA: 2017.

[33] Baker JW. Quantitative Classification of Near-Fault Ground Motions Using Wavelet Analysis. Bull Seismol Soc Am 2007;97:1486–501. https://doi.org/10.1785/0120060255.

[34] PEER. Pacific Earthquake Engineering Research Center. Ground motion database 2020. https://doi.org/https://ngawest2.berkeley.edu/.

[35] FEMA P-1051. 2015 NEHRP Recommended Seismic Provisions: Design Examples. Federal Emergency Management Agency, Washington DC: 2016.